Levitation force induced by pressure radiation in gas squeeze films

Adi Minikes[a] and Izhak Bucher[b]
Dynamics Laboratory, Faculty of Mechanical Engineering, Israel Institute of Technology, Technion, Haifa 32000, Israel

Shimon Haber[c]
Faculty of Mechanical Engineering, Israel Institute of Technology, Technion, Haifa 32000, Israel

(Received 24 July 2003; revised 7 February 2004; accepted 19 April 2004)

An analytical and numerical study on the levitation force induced by pressure radiation in gas squeeze films is investigated. The levitation phenomenon is known to occur when a planar object is placed at close proximity to a vibrating piston. The existing analytical approaches are based on either conventional acoustic radiation, where the fluid is assumed inviscid or on a variant of the Reynolds equation that incorporates viscous effects. Alas, these solutions are often in poor agreement with accurate numerical results and, at best, describe appropriately cases that include a limited range of object weights and vibration frequencies. In this work, two cases are addressed: the flow induced by vibrations perpendicular to a flat surface and that by flexural wave propagation parallel to the surface. For the first case, numerical and second-order analytical perturbation solutions are obtained and compared, proving them to be in good agreement. In addition, a novel, analytical expression for the levitation force is also suggested that proves to be valid for a wider physical range of squeeze numbers and vibration amplitudes. For the second and more complex case (recently used in noncontacting transportation systems where the driving surface exhibited flexural traveling waves), the skin-friction force exerted on the flat surface is derived analytically based on a first-order perturbation solution, and the levitation force is analyzed numerically. Some insights on the physical behavior are then highlighted and discussed.
[DOI: 10.1121/1.1760110]

PACS numbers: 43.25.Uv, 43.25.Op [MFH] Pages: 217–226

I. INTRODUCTION

The near field acoustic levitation phenomenon, where planar objects are being levitated when brought close to a vibrating piston, has been carried out by several studies in the past (e.g., Refs. 1–6). More recently, the acoustic levitation effect was applied in noncontacting linear transportation systems[7–10] where a combination of normal and lateral motions was observed. Such a combination is of fundamental importance if the transportation of objects without any direct contact with the driving surface is desired.

Normal levitation occurs when a planar target is placed in the path of an unbounded acoustic beam, the time average pressure (often referred to as the Langevin radiation pressure) exerted on the target, creates a levitation force which is related to variation in acoustic impedance with time. The levitated planar object acts as a reflector and the closer the object approaches the radiating source the larger the levitation force becomes. This is different from the conventional acoustic levitation of small objects (such as drops), where the levitation takes place near the nodes of standing pressure waves that are formed between a radiating source and a reflector.

Hashimoto *et al.*[1] provided a simplified mathematical formulation by which the levitation force based on the acoustic radiation theory presented by Chu *et al.*[2] was calculated for a one-dimensional field. Nomura *et al.*[4] numerically analyzed a two-dimensional axisymmetric pressure field, solving the continuity and momentum equations for adiabatic conditions. The disagreement between the numerical results[4] and the analytical solution[1] was attributed to energy leakages in the peripheries of the levitated object, not accounted for by the one-dimensional model.

A different approach for obtaining the pressure field was suggested by Langlois[11] who performed an order of magnitude analysis of the continuity, momentum, and energy equations to derive the nonlinear, incompressible, and isothermal Reynolds equations for the fluid layer (squeeze film) between two normal vibrating surfaces. Langlois[11] was not concerned with radiation pressure since he dealt with an incompressible medium. Salbu,[5] however, studied experimentally a compressible squeeze film and solved analytically the Reynolds equation using mass conservation across the boundaries. Such a solution introduces a discontinuity of the pressure field at the boundaries and, therefore, is limited to cases where a relatively large amount of energy is introduced into the medium, i.e., for large squeeze numbers (this will be explained in detail in the next section).

Lateral motion accompanied with normal levitation[7–10] occurs when the oscillatory motion between two surfaces, creates traveling waves. Such a lateral motion is the result of

[a]Electronic mail: minikes@technion.ac.il
[b]Author to whom correspondence should be addressed. Electronic mail: bucher@technion.ac.il
[c]Electronic mail: mersh01@tx.technion.ac.il

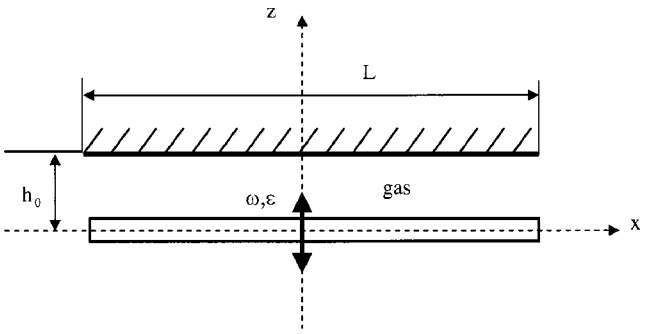

FIG. 1. Schematic layout of the problem.

wall shear stresses and the nonuniform lateral pressure gradients. Since the shear forces are related to the viscosity of the medium, acoustic theories for inviscid fluids must be accompanied with the theory of acoustic streaming.

In the present paper, we begin with a brief discussion of the Reynolds equation, examine previous solutions, and discuss their restrictions. Next, we study an analytical solution for the radiation pressure generated by the normal vibration of a flat piston. A perturbation approach is used, in combination with the mass conservation equation. Finally, we investigate the case which incorporates a driving surface that includes flexural traveling waves. A first-order perturbation scheme is used to obtain the shear stresses force exerted on the surface, whereas for the levitation force a numerically study is performed.

II. STATEMENT OF THE PROBLEM

Consider the case illustrated in Fig. 1 where a flat surface is placed at a mean distance h_0 from a flat plane of width (L) and of a much larger length. The driving surface oscillates at a frequency ω and amplitude $\varepsilon h_0(\varepsilon<1)$. The vibrating surface squeezes the compressible fluid that occupies the clearance between the planes, generating a time average pressure higher than the surrounding. This load-carrying phenomenon arises from the fact that the viscous flow is not instantaneously squeezed out from the clearance giving rise to a cushioning effect.

The nondimensional Reynolds number could be estimated by $\mathrm{Re}=\rho\omega h_0^2/\mu$. For typical values (in M.K.S. units) of the physical parameters in this problem density $\rho \approx O(1)$, $\omega\approx O(10^4)$, $h_0\approx O(10^{-5})$, and viscosity $\mu \approx O(10^{-5})$, the Reynolds number is of order $\mathrm{Re} \approx O(10^{-1})$, suggesting that the fluid inertia is negligible in comparison to viscous forces.

The fluid velocity normal to the surfaces is of the order of $h_0\varepsilon\omega$ and the fluid velocity tangent to the surface is of order $L\omega\varepsilon$. Hence, since $L\gg h_0$, the normal velocity is negligibly small compared with the gas velocity in the lateral direction. Performing an order of magnitude analysis, the differential momentum equation reveals that the pressure gradient in the normal direction is of order h_0/L, which is much smaller than that in the lateral direction (order unity) and, as a consequence, the pressure gradient in the normal direction can be neglected.

We further assume that the squeezed film is isothermal. The latter is a reasonable assumption since the gas film is very thin and of low heat capacity when compared with that of the bearing surfaces. The characteristic time of temperature variations across the squeezed film is approximately given by $t\approx h_0^2/\alpha\approx O(10^{-5}[\mathrm{s}])$ where α is the thermal diffusivity of the gas. This characteristic time is an order of magnitude shorter than that of the periodic oscillation time $1/\omega=O(10^{-4}[\mathrm{s}])$. Therefore the temperature field is nearly uniform across the squeezed film during each time cycle. Moreover, if the bounding surfaces are of uniform temperature, the whole fluid occupying the space between the plates is isothermal.

Integrating the continuity equation across the film thickness and substituting the velocity profile into the momentum equation results in the governing one-dimensional, time-dependent Reynolds equation for laminar, Newtonian, isothermal, and compressible thin film flow:[12]

$$\frac{\partial}{\partial X}\left(H^3P\frac{\partial P}{\partial X}\right)=\sigma\frac{\partial}{\partial T}(PH), \tag{1}$$

where

$$P=\frac{p}{p_a},\quad H=\frac{h}{h_0},\quad X=\frac{x}{L},\quad T=\omega t,\quad \sigma=\frac{12\omega\mu L^2}{p_a h_0^2}.$$

Here, P_a is the ambient pressure, P, H, X, and T are the dimensionless pressure, mean clearance, lateral coordinate, and time, respectively, and σ stands for the squeeze number.

III. FLAT DRIVING SURFACE

Assume that the clearance between the surfaces illustrated in Fig. 1 varies with time according to

$$H(T)=1+\varepsilon\cos(T). \tag{2}$$

Langlois[11] solved Eq. (1) assuming that the pressure field can be expanded as a regular perturbation series in ε:

$$P(X,T)=1+\varepsilon\Pi(X,T)+O(\varepsilon^2). \tag{3}$$

Substituting Eqs. (2) and (3) into Eq. (1) and neglecting terms of order higher than ε^2 results in a linear, inhomogeneous diffusion equation of the form

$$\frac{\partial\Pi}{\partial T}=\frac{1}{\sigma}\frac{\partial^2\Pi}{\partial X^2}+\sin(T)+O(\varepsilon^2). \tag{4}$$

Subjected to ambient pressure ($P=1$) at the initial and boundary conditions,

$$\text{I.C.:}\quad \Pi(X,T=0)=0,\quad \text{B.C.:}\quad \Pi(X=\pm 0.5,T)=0,$$

a steady-state solution of Eq. (4) that oscillates with the excitation frequency is

$$\Pi(X,T)=\Pi_1(X)\cos(T)+\Pi_2(X)\sin(T). \tag{5}$$

Substituting Eq. (5) solution into Eq. (4) and collecting similar terms yields

$$\left(\sigma\Pi_2-\frac{\partial^2\Pi_1}{\partial X^2}\right)\cos(T)=\left(\sigma\Pi_1+\frac{\partial^2\Pi_2}{\partial X^2}+\sigma\right)\sin(T). \tag{6}$$

Since the foregoing equation should hold for all values of T, both sides must vanish identically and Π_1 and Π_2 vanish at $X=\pm 0.5$. Thus, Π_1 and Π_2 are determined by a pair of

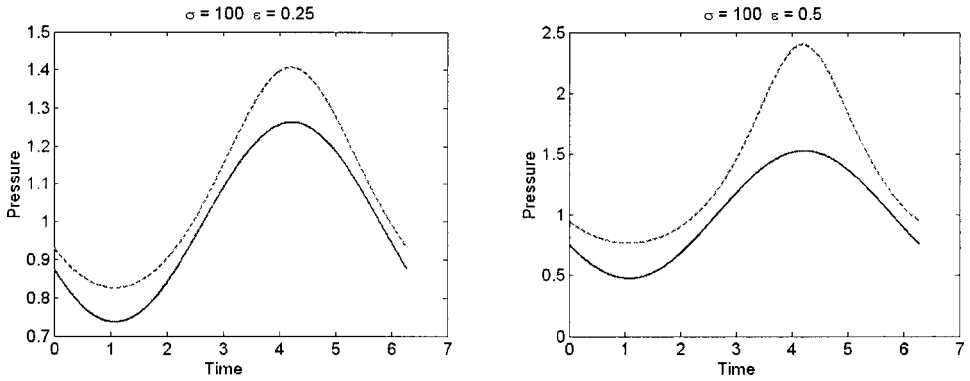

FIG. 2. Pressure change during one time period at the center of the plate; Eq. (6) and the numerical solution are shown by solid and dashed lines, respectively. (a) $\sigma=100$, $\varepsilon=0.25$ and (b) $\sigma=100$, $\varepsilon=0.5$.

coupled differential equations whose solution is[11]

$$\Pi_1(X)=\frac{2}{\cosh(\beta)+\cos(\beta)}\left[\cosh\left(\frac{\beta}{2}\right)\cos\left(\frac{\beta}{2}\right)\cosh(\beta X)\times\cos(\beta X)+\sinh\left(\frac{\beta}{2}\right)\sin\left(\frac{\beta}{2}\right)\times\sinh(\beta X)\sin(\beta X)\right]-1, \tag{7a}$$

$$\Pi_2(X)=\frac{2}{\cosh(\beta)+\cos(\beta)}\left[\sinh\left(\frac{\beta}{2}\right)\sin\left(\frac{\beta}{2}\right)\cosh(\beta X)\times\cos(\beta X)-\cosh\left(\frac{\beta}{2}\right)\cos\left(\frac{\beta}{2}\right)\sinh(\beta X)\sin(\beta X)\right], \tag{7b}$$

where $\beta=\sqrt{\sigma/2}$.

A comparison between this solution [Eq. (5)] and a numerical solution of the Reynolds equation [Eq. (1)] is plotted in Fig. 2. It shows how the pressure at the center of the wall varies over a single time period for two different values of ε. Equation (1) was solved numerically by means of a second-order central-finite differences in space and adaptive time integration.[10] The plots reveal that the solutions are in phase. However, while the numerically calculated average pressure is greater than unity, the analytically approximated one equals exactly to unity (i.e., equals to the ambient pressure). As expected, the numerical solution suggests that the squeeze film levitation phenomenon is related to nonlinear effects associated with higher-order terms of the perturbation solution. The pressure oscillations, obtained numerically, which are not pure cosine functions, also suggest that the solution consists of higher harmonics of the excitation frequency. The differences between the numerical and the analytical solutions decrease as the vibration amplitude (ε) is decreased. Obviously, in the presence of small vibration amplitudes, less energy is delivered into the system and the squeeze effect barely takes place.

Instead of finding the pressure distribution in time and space we could search for a weaker solution by integrating the governing equation with respect to time and space. Salbu[5] utilized this methodology investigating the case of a flat driving surface oscillating in the normal direction. He showed that gaseous squeezed films behave as if they were incompressible at the boundaries and solely compressible in the interior. The size of the interior region increases from zero to the full wall width as σ increases. The interior region behaves like a spring (the pressure in phase with the vibration displacement) and the exterior region behaves like a damper (the pressure becomes proportional to the vibration velocity). Such behavior of a phase shift in the pressure along the film is associated with the energy leakage at the boundaries. Figure 3 shows numerical results of the pressure distribution along the wall as it varies over a time period.

The contours in Fig. 3 represent isobars in the film. The curvature of contours illustrates the phase shift in pressure along the wall. Observing the pressure gradients along the wall indicates that the gas flow takes place mostly near the boundaries, alternating between inward and outward directions. Comparing the two figures 3(a) and 3(b) confirms that the interior region increases with the increase of the squeeze

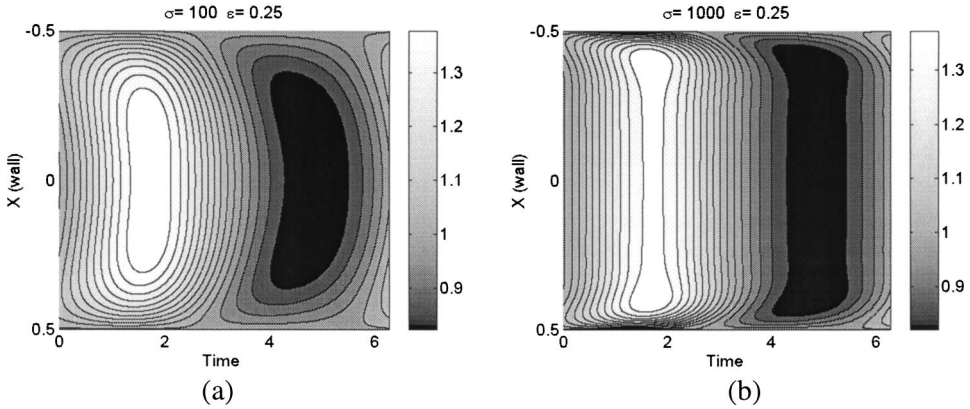

FIG. 3. Numerical results of the pressure distribution along the wall as it varies over a time period for two different squeeze numbers: (a) $\sigma=100$, $\varepsilon=0.25$ and (b) $\sigma=1000$, $\varepsilon=0.25$.

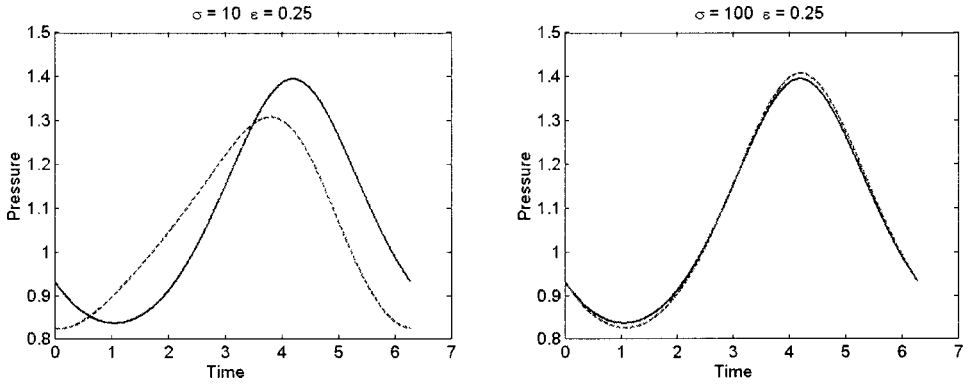

FIG. 4. Change of pressure at the center of the wall during a single time period as obtained by Eq. (12) (solid curves) and numerically (dashed curves): (a) $\sigma=10$, $\varepsilon=0.25$ and (b) $\sigma=100$, $\varepsilon=0.25$.

number and the phase shift in the pressure begins at a closer region to the boundaries.

At high squeeze numbers, virtually no flow occurs at the peripheries of the wall, and the system mimics that of a piston in a closed channel. In such a case and under the isothermal condition assumption, mass conservation yields $PH=C=\text{const}$ [the term $\sigma\partial(PH)/\partial T$ must remain bounded when $\sigma\to\infty$]. This assumption violates the boundary conditions since it introduces a discontinuity in the pressure field. Under this assumption, integrating both sides of Eq. (1) over a time period yields[5]

$$\int_0^{2\pi}\frac{\partial}{\partial X}\left(H^3P\frac{\partial P}{\partial X}\right)dT=\sigma\int_0^{2\pi}\frac{\partial}{\partial T}(PH)\,dT=0. \tag{8}$$

Further integrating with respect to X (from X to $X=0$) reduces the equation to

$$\left[\int_0^{2\pi}H^3P\frac{\partial P}{\partial X}dT\right]_x=\left[\int_0^{2\pi}H^3P\frac{\partial P}{\partial X}dT\right]_{x=0}=\text{const}. \tag{9}$$

Thus, Eq. (9) holds for all values of X. Owing to system's symmetry, the pressure gradient at the center of the wall satisfies the condition $\partial P/\partial X=0$ and, thereby, the constant in Eq. (9) must vanish. Integrating Eq. (9) once again with respect to X (from X to $X=\frac{1}{2}$) yields

$$\left[\int_0^{2\pi}H^3P^2\,dT\right]_x=\left[\int_0^{2\pi}H^3P^2\,dT\right]_{x=1/2}=\text{const}. \tag{10}$$

Since practically no flow takes place at the peripheries of the wall, the assumption of nonleakage of energy permits us to utilize a pressure release boundary condition ($P=1$), and the constant on the rhs of Eq. (10) becomes

$$\text{const}=\int_0^{2\pi}H^3\,dT=\int_0^{2\pi}[1+\varepsilon\cos(T)]^3dT=\pi(2+3\varepsilon^2). \tag{11}$$

Since $PH=C$, where C is determined from Eq. (10) by solving $C^2\int_0^{2\pi}H\,dT=\pi(2+3\varepsilon^2)$, the pressure possesses the form

$$P=\frac{C}{H}=\frac{(1+\frac{3}{2}\varepsilon^2)^{1/2}}{1+\varepsilon\cos(T)}. \tag{12}$$

This mass conservation solution obtained by Salbu[5] is not only independent of the squeeze number σ but also does not incorporate the pressure distribution along the wall. Therefore it would be suitable for cases with large squeeze numbers. An example for realizing the values of such high squeeze numbers is, for instance, the squeeze number for standard atmospheric air under vibration frequency $\omega=4\pi\times10^4$ (rad/s) with a mean clearance $h_0=50\,(\mu\text{m})$ and a bearing width $L=0.1\,(\text{m})$ which results in $\sigma=1000$.

A comparison between this analytical solution [Eq. (12)] and a numerical solution of the governing equation is plotted in Fig. 4, where the change of pressure with time at the center of the wall (at steady state) for two different squeeze numbers is presented. Figure 4 suggests that Salbu's analytical solution for the pressure at the center of the wall, where relative large squeeze numbers exist, correlates well with our numerical solutions. However, examination of the numerical results of the maximum pressure distribution along the wall for different squeeze numbers (as illustrated in Fig. 5) clearly demonstrates that the assumption $PH=\text{const}$ is valid only for high squeeze numbers where the pressure distribution becomes nearly uniform. Under a vibration amplitude of $\varepsilon=0.25$, the maximum pressure value obtained by Eq. (12) is $P=1.395$. This value is plotted in Fig. 5 together with the numerical results.

The estimation of the pressure distribution in Eq. (12) could be enhanced by edge corrections that would satisfy the boundary conditions. Equation (12) assumes uniform pressure distribution along the wall, independent of the squeeze number. On the other hand, the first-order perturbation solu-

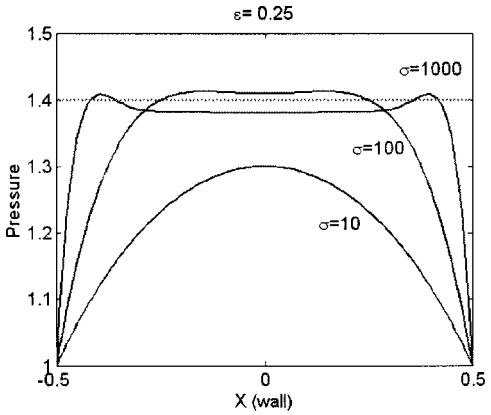

FIG. 5. Numerical results obtained by Eq. (1) for the maximum pressure distribution along the wall for various squeeze numbers (solid curves), and the maximum pressure obtained by Eq. (12) (dotted curve). Here $H(T)=1+0.25\cos(T)$.

tion, Eq. (5), offers an adequate approximation for the relative pressure distribution along the wall at a given moment in time. Consequently, we suggest correcting the conservation mass solution in the following manner:

$$P=1+\left(\frac{(1+\frac{3}{2}\varepsilon^2)^{1/2}}{1+\varepsilon\cos(T)}-1\right)\underset{x}{\mathrm{MAX}}\{\Pi(X,T)\}. \tag{13}$$

The operator MAX means that one should take the largest enveloped shape within the time period. The enveloped shape is, obviously, not time independent but, while time differences may be significant, the value of Eq. (12) is negligibly affected. In order to find this enveloped shape one must find the time $T_{\max}$ where the pressure amplitude is maximal. It appears that for squeeze numbers greater than 20 the two solutions are in phase, therefore allowing us to find the time $T_{\max}$ by solving

$$\frac{\partial}{\partial T}P(T)=\frac{\partial}{\partial T}\left(\frac{(1+\frac{3}{2}\varepsilon^2)^{1/2}}{1+\varepsilon\cos(T)}\right)=0\Rightarrow T_{\max}=\pi. \tag{14}$$

Substituting $T_{\max}=\pi$ into Eq. (5) yields the maximum enveloped shape and consequently the rectified mass conservation solution possesses the form

$$P=1+\left(\frac{(1+\frac{3}{2}\varepsilon^2)^{1/2}}{1+\varepsilon\cos(T)}-1\right)\left(1-2\,\frac{\cosh(\beta/2)\cos(\beta/2)\cosh(\beta X)\cos(\beta X)+\sinh(\beta/2)\sin(\beta/2)\sinh(\beta X)\sin(\beta X)}{\cosh(\beta)+\cos(\beta)}\right). \tag{15}$$

Our proposed correction allows solving analytically the levitation force for a larger range of squeeze numbers than was initially offered by Eq. (12). The dimensionless time averaged levitation force (W) per unit depth at steady state can be expressed by

$$W=\frac{1}{2\pi}\int_0^{2\pi}\int_{-1/2}^{1/2}(P-1)\,dX\,dT, \tag{16}$$

where W is normalized by p_aL.

Figure 6 confirms the agreement between the levitated forces obtained by Eq. (16) and the numerical solution over a large range of the squeeze number. In essence, we have obtained a good agreement between the two solutions for relatively small squeeze numbers in the range where Eq. (12) does not hold. Furthermore, the corrected solution [Eq. (15)] holds for relatively large amplitudes (ε) while the second-order perturbation solution does not (as will be shown next).

So far, we have shown that the first order perturbation solution cannot predict the levitation force. A second-order solution, accounting for nonlinear effects, may be more successful. Assume that the deviation from the ambient pressure is expanded up to order ε^2 terms as follows,

$$P(X,T)=1+\varepsilon\Pi_A(X,T)+\varepsilon^2\Pi_B(X,T)+O(\varepsilon^2). \tag{17}$$

Substituting Eq. (17) together with $H(T)=1+\varepsilon\cos(T)$ into Eq. (1) gives

$$\sigma\frac{\partial\Pi_A}{\partial T}=\frac{\partial^2\Pi_A}{\partial X^2}+\sigma\sin(T)+O(\varepsilon^2), \tag{18a}$$

$$\sigma\frac{\partial\Pi_B}{\partial T}=\frac{\partial^2\Pi_B}{\partial X^2}+G(\Pi_A)+O(\varepsilon^3), \tag{18b}$$

with

$$\text{I.C.:}\quad \Pi_{A,B}(X,T=0)=0,\quad \text{B.C.:}\quad \Pi_{A,B}(X=\pm 0.5,T)=0,$$

where the forcing term of Eq. (18b) possesses the simplified form

$$G(\Pi_A)=\frac{1}{\sigma}\left(\frac{\partial\Pi_A}{\partial X}\right)^2+\frac{\partial\Pi_A}{\partial T}[\Pi_A+2\cos(T)]-\frac{3}{2}\sin(2T). \tag{19}$$

Substituting the first-order perturbation solution Eq. (5) into Eq. (19) results in an expression of the following form:

$$G(\Pi_A)=G_1(X)\cos(2T)+G_2(X)\sin(2T)+A(X), \tag{20}$$

where $G_1(X)$, $G_2(X)$ and $A(X)$ are known functions of X.

A steady-state harmonic solution based on Eq. (20) is

$$\Pi_B(X,T)=\Pi_3(X)\cos(2T)+\Pi_4(X)\sin(2T)+\Pi_5(X). \tag{21}$$

Substituting this solution into Eq. (18b) and performing harmonic balancing results in

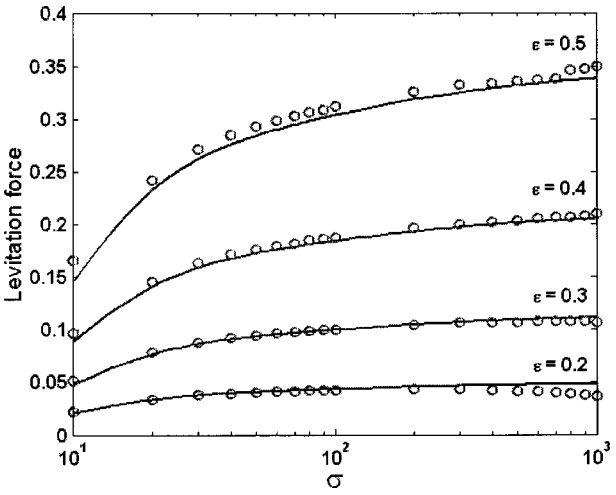

FIG. 6. Time averaged levitation force versus squeeze number (σ) for different vibration amplitudes (ε). Solid curves—Eq. (16). Circles—numerical solution.

$$\left(2\sigma\Pi_4-\frac{\partial^2\Pi_3}{\partial X^2}+\sigma G_1(X)\right)\cos(2T)$$
$$=\left(2\sigma\Pi_3+\frac{\partial^2\Pi_4}{\partial X^2}+\sigma G_2(X)\right)\sin(2T)$$
$$+\left(\frac{\partial^2\Pi_5}{\partial X^2}+A(X)\right). \tag{22}$$

Integrating over a time period, the lhs and the first term on the rhs vanish. The second term on the rhs is not a function of time and, therefore, must vanish identically:

$$\frac{\partial^2\Pi_5}{\partial X^2}+A(X)=0, \quad \text{B.C.:} \quad \Pi_5(X=\pm 0.5,T)=0. \tag{23}$$

A solution of Eq. (23) would eventually provide the difference between the time-averaged pressure in the squeeze film and the ambient pressure. The solution for $\Pi_5(X)$ is given by

$$\Pi_5(X)=\frac{1}{4\cos(\beta)+4\cosh(\beta)}\left[5\cosh(\beta)+5\cos(\beta)\right.$$
$$-\cosh(2\beta X)-\cos(2\beta X)-4\cos\left(\beta X-\frac{\beta}{2}\right)$$
$$\times\cosh\left(\beta X+\frac{\beta}{2}\right)-4\cos\left(\beta X+\frac{\beta}{2}\right)$$
$$\left.\times\cosh\left(\beta X-\frac{\beta}{2}\right)\right]. \tag{24}$$

Utilizing Eq. (16), the time-averaged levitation force per unit depth is

$$W=\frac{1}{2\pi}\int_0^{2\pi}\int_{-1/2}^{1/2}(P-1)dX\,dT=\int_{-1/2}^{1/2}\varepsilon^2\Pi_5(X)dX, \tag{25}$$

$$W=\frac{5\varepsilon^2}{4\beta}\left[\frac{\beta\cos(\beta)+\beta\cosh(\beta)-\sinh(\beta)-\sin(\beta)}{\cos(\beta)+\cosh(\beta)}\right].$$

Figure 7 compares between the time-averaged levitation forces obtained by Eq. (25) and that of the rectified mass conservation solution [Eq. (16)]. It shows that for vibration amplitudes, up to about one-third of the mean gap, the second-order perturbation solution and the corrected mass solution are in good agreement. As expected, with the increase of the vibration amplitude (ε), the agreement deteriorates since third-order terms are no longer negligible and the differences can reach up to 12% for $\varepsilon=0.5$.

IV. TRAVELING WAVE VIBRATIONS

Let us now consider a more complex case illustrated in Fig. 8 where a kinematical flexural traveling wave is brought closely to a wall of width (L) and its (y direction) length is much larger than its width. The traveling wave propagates in the positive x direction with uniform amplitude along the y direction (which is much larger than L), oscillating at frequency (ω), possessing an amplitude (ε) and wavelength (λ).

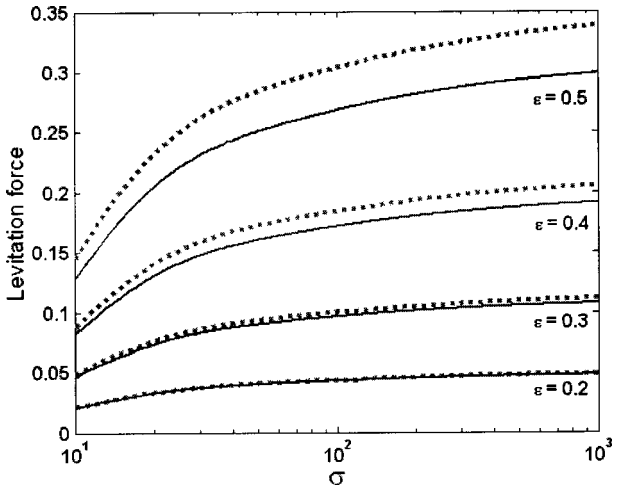

FIG. 7. Time averaged levitation force versus squeeze number (σ) for different vibration amplitudes (ε). Solid curve—Eq. (25). Dotted curves—Eq. (16) with Eq. (15).

The sound field generated by the traveling wave produces two forces acting on the wall surface: the acoustic radiation force acting in the normal direction and the shear force acting in the tangential direction. The viscous shear force results from the gradients in the acoustic streaming velocity at the viscous boundary layer adjacent to the wall surface. This case is of fundamental importance in analyzing noncontacting transportation mechanisms. It is worth distinguishing between the boundary conditions created by a moving wavy surface and a surface experiencing flexural traveling wave. While in the first case, a material point propagates laterally with the surface, in the latter, a material point vibrates in a direction perpendicular to the wave propagation. Consequently, in the case of flexural traveling waves, lateral velocity of the fluid along the wall is a direct result of pressure gradients only. In this case, the clearance between surfaces can be described by

$$H(X,T)=1+\varepsilon\cos(T-kX), \tag{26}$$

where $k=2\pi L/\lambda$ denotes the dimensionless wave number.

A first-order solution is obtained in a similar fashion to that shown in the previous section, namely, assuming that the pressure possesses a regular expansion in ε $P(X,T)=1$

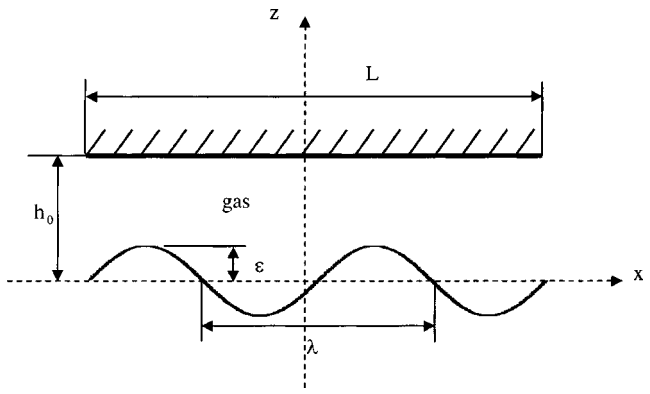

FIG. 8. Schematic layout of the problem.

$+\varepsilon\Pi(X,T)+O(\varepsilon^2)$. The resulting differential equation for the first-order perturbation function Π is a linear, inhomogeneous diffusion equation of the form

$$\frac{\partial \Pi}{\partial T}=\frac{1}{\sigma}\frac{\partial^2 \Pi}{\partial X^2}+\sin(T-kX)+O(\varepsilon^2) \tag{27}$$

subjected to the following initial and boundary conditions,

$$\text{I.C.:}\quad \Pi(X,T=0)=0,\quad \text{B.C.:}\quad \Pi(X=\pm 0.5,T)=0.$$

Again we assume that a steady-state solution of Eq. (27) varies harmonically in time, oscillating with the excitation frequency:

$$\Pi(X,T)=\Pi_1(X)\cos(T)+\Pi_2(X)\sin(T). \tag{28}$$

Substituting Eq. (28) into Eq. (27) and collecting similar terms in time yields

$$\left(\sigma\Pi_2-\frac{\partial^2\Pi_1}{\partial X^2}+\sigma\cos(kX)\right)\cos(T)$$

$$=\left(\sigma\Pi_1+\frac{\partial^2\Pi_2}{\partial X^2}+\sigma\sin(kX)\right)\sin(T). \tag{29}$$

Since Eq. (29) is valid for all values of T, the terms in the (large) parenthesis must vanish identically. Similarly, the boundary conditions are that both Π_1 and Π_2 vanish at $X=\pm 0.5$. Thus, Π_1 and Π_2 are determined by the following pair of coupled differential equations

$$\frac{\partial^2\Pi_1}{\partial X^2}-\sigma\Pi_2-\sigma\sin(kx)=0, \tag{30a}$$

$$\frac{\partial^2\Pi_2}{\partial X^2}+\sigma\Pi_1+\sigma\cos(kx)=0, \tag{30b}$$

and boundary conditions

$$\text{B.C.:}\quad \Pi_1(X=\pm 0.5,T)=\Pi_2(X=\pm 0.5,T)=0.$$

Equations (30a) and (30b) can be combined into a single second-order equation of the complex variable $\Phi=(\Pi_1-i\Pi_2)$ with boundary conditions $\Phi(X=\pm 0.5,T)=0$. The solution of Φ possesses the general form

$$\Phi=\frac{2\beta^2}{i2\beta^2+k^2}\left(\frac{\sin(k/2)\sin(\beta X-i\beta X)}{\sin((\beta-i\beta)/2)}-\sin(kX)\right.$$
$$\left.+\frac{i\cos(k/2)\cos(\beta X-i\beta X)}{\cos([\beta-i\beta]/2)}-i\cos(kX)\right), \tag{31}$$

where here, as before, $\beta=\sqrt{\sigma/2}$ and $i=\sqrt{-1}$.

Equation (31) degenerates into Eqs. (7a) and (7b) when setting the wavelength to infinity ($k\to 0$) and thus serves as a generalization of the results in Ref. 11. The first-order perturbation solution in Eq. (31) is valid for incompressible fluids and for low squeeze numbers (as compressibility effects are negligible). This solution may be rewritten in the form

$$\Pi_1(X)=\Phi_1\sin(\beta X)\cosh(\beta X)+\Phi_2\cos(\beta X)\sinh(\beta X)$$
$$+\Phi_3\cos(\beta X)\cosh(\beta X)$$
$$+\Phi_4\sin(\beta X)\sinh(\beta X)+\Phi_5\cos(kX)$$
$$+\Phi_6\sin(kX), \tag{32a}$$

$$\Pi_2(X)=-\Phi_2\sin(\beta X)\cosh(\beta X)+\Phi_1\cos(\beta X)$$
$$\times\sinh(\beta X)+\Phi_4\cos(\beta X)\cosh(\beta X)$$
$$-\Phi_3\sin(\beta X)\sinh(\beta X)-\Phi_6\cos(kX)$$
$$+\Phi_5\sin(kX), \tag{32b}$$

where

$$\Phi_1=\frac{2\beta^2}{\Delta_1}\left[k^2\sin\left(\frac{\beta}{2}\right)\cosh\left(\frac{\beta}{2}\right)\right.$$
$$\left.+2\beta^2\cos\left(\frac{\beta}{2}\right)\sinh\left(\frac{\beta}{2}\right)\right]\sin\left(\frac{k}{2}\right),$$

$$\Phi_2=\frac{2\beta^2}{\Delta_1}\left[k^2\cos\left(\frac{\beta}{2}\right)\sinh\left(\frac{\beta}{2}\right)\right.$$
$$\left.-2\beta^2\sin\left(\frac{\beta}{2}\right)\cosh\left(\frac{\beta}{2}\right)\right]\sin\left(\frac{k}{2}\right),$$

$$\Phi_3=\frac{2\beta^2}{\Delta_2}\left[2\beta^2\cos\left(\frac{\beta}{2}\right)\cosh\left(\frac{\beta}{2}\right)\right.$$
$$\left.+k^2\sin\left(\frac{\beta}{2}\right)\sinh\left(\frac{\beta}{2}\right)\right]\cos\left(\frac{k}{2}\right),$$

$$\Phi_4=\frac{2\beta^2}{\Delta_2}\left[2\beta^2\sin\left(\frac{\beta}{2}\right)\sinh\left(\frac{\beta}{2}\right)\right.$$
$$\left.-k^2\cos\left(\frac{\beta}{2}\right)\cosh\left(\frac{\beta}{2}\right)\right]\cos\left(\frac{k}{2}\right),$$

$$\Phi_5=-\frac{4\beta^4}{4\beta^4+k^4},\quad \Phi_6=-\frac{2\beta^2k^2}{4\beta^4+k^4},$$

$$\Delta_1=(4\beta^4+k^4)\left[\cosh\left(\frac{\beta}{2}\right)^2-\cos\left(\frac{\beta}{2}\right)^2\right],$$

$$\Delta_2=(4\beta^4+k^4)\left[\cosh\left(\frac{\beta}{2}\right)^2+\cos\left(\frac{\beta}{2}\right)^2-1\right].$$

Figures 9(a) and 9(b) compares an example of pressure distribution along the wall over one time period obtained by the first-order solution in Eq. (32) and a numerical solution of Eq. (1). The inclination angle of the contours in Figs. 9(a) and 9(b) are formed as a result of the wave propagation. This inclination angle will decrease with the increase of the wavelength (increase of the propagation velocity of the wave) until it reaches the field described in Fig. 3(a). The plots in Figs. 9(a) and 9(b) are for a flexural wave, traveling from $X=-0.5$ to $X=0.5$. It is clearly seen that the absolute pressure values increase along the wall in the direction of the traveling wave, therefore introducing a moment on the wall. Furthermore, while the nominal values of the pressure field in Fig. 9(b) are slightly higher than those shown in Fig. 9(a), due to the pressure radiation, the pressure gradients along the wall are comparable, suggesting that the first-order solution may offer a good approximation for the pressure distribution along the wall. The shear stresses experienced in the flow are proportional to the lateral pressure gradients. Hence we seek to obtain an approximated analytical expression for the shear

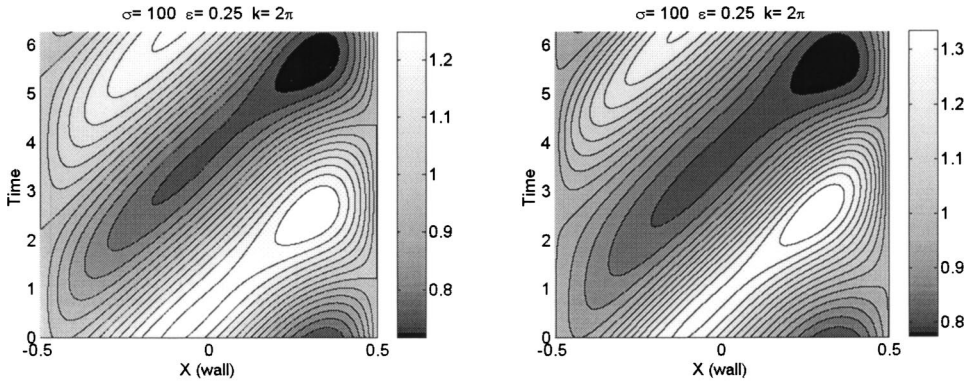

FIG. 9. Pressure distribution along the wall over one time period for $\sigma=100$, $\varepsilon=0.25$, $k=2\pi$. (a) First-order solution Eq. (32). (b) Numerical solution of Eq. (1).

stress exerted on the wall, based on the pressure first-order solution.

Solving the momentum equation in the X direction, assuming that the inertia terms can be neglected and that the velocity adheres to the walls, yields

$$v_x=\frac{z}{2\mu}\frac{\partial p}{\partial x}(z-h). \tag{33}$$

The shear stress on the wall becomes

$$\tau_{zx}|_{z=h}=\mu\left.\frac{\partial v_x}{\partial z}\right|_{z=h}=\frac{h}{2}\frac{\partial p}{\partial x} \tag{34}$$

and the dimensionless time averaged shear force per unit depth exerted on the wall at steady state is

$$F=-\frac{1}{2\pi}\int_0^{2\pi}\int_0^1 H\frac{\partial P}{\partial X}dX\,dT. \tag{35}$$

Here, F is normalized by $h_0p_a/2$.

Substituting Eq. (3) together with Eqs. (5) and (32) into Eq. (35) derives the first-order solution for the time average shear force on the wall (F) as a function of wave number, squeeze number, and vibration amplitude:

$$F=\frac{-\varepsilon^2}{16\beta^4+4k^4}\left\{\left[C_1\sin\left(\frac{\beta}{2}\right)\sinh\left(\frac{\beta}{2}\right)+C_2\cos\left(\frac{\beta}{2}\right)\times\cosh\left(\frac{\beta}{2}\right)\right]\sin\left(\frac{k}{2}\right)+\left[C_3\cos\left(\frac{\beta}{2}\right)\sinh\left(\frac{\beta}{2}\right)+C_4\sin\left(\frac{\beta}{2}\right)\cosh\left(\frac{\beta}{2}\right)\right]\cos\left(\frac{k}{2}\right)+C_5\right\}, \tag{36}$$

where

$$C_1=(8\beta^3k+4\beta k^3)\Phi_1+(8\beta^3k-4\beta k^3)\Phi_2-16\beta^4\Phi_3-8\beta^2k^2\Phi_4,$$

$$C_2=(4\beta k^3-8\beta^3k)\Phi_1+(8\beta^3k+4\beta k^3)\Phi_2-8\beta^2k^2\Phi_3+16\beta^4\Phi_4,$$

$$C_3=8\beta^2k^2\Phi_1+16\beta^4\Phi_2+(4\beta k^3-8\beta^3k)\Phi_3-(8\beta^3k+4\beta k^3)\Phi_4,$$

$$C_4=16\beta^4\Phi_1-8\beta^2k^2\Phi_2+(8\beta^3k+4\beta k^3)\Phi_3+(4\beta k^3-8\beta^3k)\Phi_4,$$

$$C_5=2k^5\Phi_6+8k\beta^4\Phi_5.$$

Comparison between the time-averaged shear force obtained analytically with Eq. (36) and the one obtained numerically by solving Eq. (1) is presented in Fig. 10. The plot shows an agreement between the solutions for different vibration amplitudes (ε) as a function of the wave number (k) for squeeze number $\sigma=100$. The results confirm that for cases where the vibration amplitudes do not exceed about one-third of the mean clearance ($\varepsilon=0.3$), the first-order perturbation solution provides a good approximation for the time-averaged shear force.

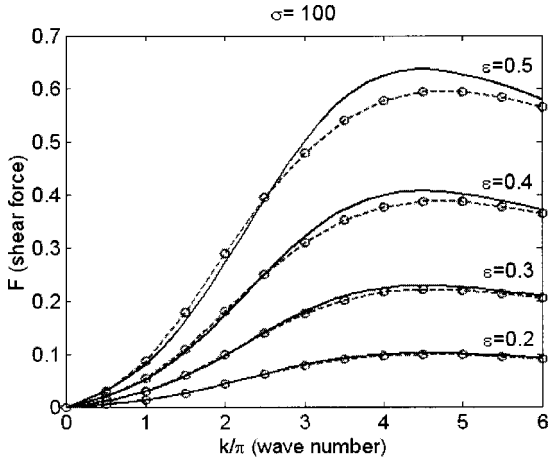

FIG. 10. Time averaged shear force exerted on the wall as function of the wave number for different vibration amplitudes, obtained analytically (solid curves) and numerically (circles). Here $\sigma=100$.

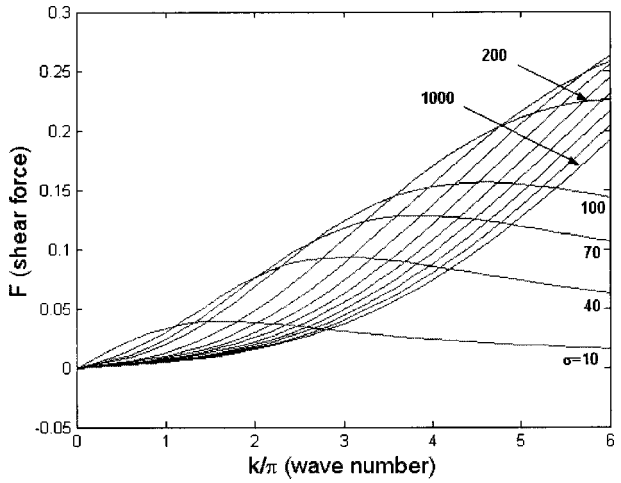

FIG. 11. Shear force exerted on the wall as a function of the wave number (k) for different values of squeeze numbers (σ), obtained by Eq. (36) provided $H(X,T)=1+0.25\cos(T-kX)$.

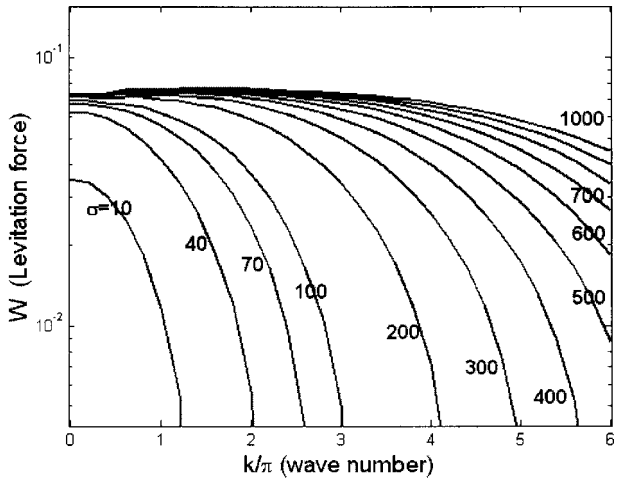

FIG. 12. Numerical results of the change of levitation force (W) with the increase of the wave number (k) for different values of squeeze numbers (σ) with $H(X,T)=1+0.25\cos(T-kX)$.

Figure 11 depicts the dependence of time-averaged shear force on the wave number, for various values of squeeze numbers and for wave amplitude $\varepsilon=0.25$. It manifests that each curve pertaining to a particular squeeze number possesses a maximum that shifts up and to the right with an associated increase of the squeeze number. That a maximum value must exist can be explained by examining the behavior at two extreme cases. When the wave number is zero, the pressure along the wall is symmetric with respect to the surface center and, consequently, no net shear force is exerted. On the other hand, when the wave number approaches infinity, the velocity of the propagating wave approaches to zero and the driving surface is nearly symmetric (with respect to the center), once again no net shear force is being generated.

Trying to enhance our solution by adding a second-order perturbation requires tedious manipulations of very long analytical expressions in trying to solve Eq. (23) for $\Pi_5(X)$. Consequently, this approach loses its appeal as a vehicle for gaining a better understanding of the governing parameters. Alternatively, we may apply the mass conservation method in a manner similar to that of the former case, resulting in

$$P=\frac{C}{H}=\frac{(1+\frac{3}{2}\varepsilon^2)^{1/2}}{1+\varepsilon\cosh(T-kX)}. \tag{37}$$

Although this solution depends explicitly on X and the wave number, the mean levitation force over a time period depends only on (ε), since the term kX is merely a phase shift. Therefore, Eq. (37) can only account for the case of traveling waves for extremely large values of σ(over 5000).

A numerical study was performed for the levitation force introduced by pressure radiation. Figure 12 presents the change of levitation force with wave number for different values of squeeze numbers and for a wave amplitude $\varepsilon=0.25$. It clearly shows that as the wave number increases (or the wave length decreases), the levitation force decreases. This is reasonable since while some regions experience compression others experience expansion, thus reducing the effective squeeze area.

The last two figures suggest that one may encounter difficulties when attempting to optimize the working parameters that would yield a maximum shear force together with a maximum levitation force. It appears that the maximum shear force on the wall occurs at wave numbers larger than those able to sustain significant levitation force for a given squeeze number.

V. CONCLUSIONS

The pressure field between a wall and a near-vibrating surface was investigated in order to obtain expressions for the pressure radiation and the shear forces acting on the wall. A novel and concise analytical expression for the time-averaged levitation force was developed and was shown to be more suitable over a wider range of squeeze numbers and vibration amplitudes than that obtained by a second-order perturbation solution. In the presence of flexural traveling waves, a first-order perturbation solution for the time-averaged shear force exerted on the wall was derived, proving to be suitable in cases where the wave amplitude does not exceed one-third of the mean clearance. Analysis of the shear-force reveals a maximum value, which depends on the wave number and the squeeze number. For this maximum shear force, at a given squeeze number, the levitation force becomes insignificant, hence, one is forced to use an intermediate operational range for simultaneous levitation and transportation. Numerical results show that the larger the wave number, the more energy is required (large squeeze numbers) for sustaining significant levitation force. In search for an analytical solution, the levitated object was considered as a rigid clamped wall in order to avoid the coupling of the object's dynamical equations with the Reynolds equation. In practice, for flat driving surfaces, according to experimental and numerical results,[4,6] this assumption holds as the vibration amplitudes of the levitated object are two orders of magnitude smaller than those of the driving surface. However, in the presence of flexural traveling waves, this assumption may not be valid since alternating moments, induced by the film, may cause the levitated object to tilt harmonically

around an average attack angle while propagating.[10] Still, we believe that the presented analysis clarifies the physical mechanisms underling the levitation phenomena in the presence of traveling waves.

[1] Y. Hashimoto, Y. Koike, and S. Ueha, ''Near-field acoustic levitation of planar specimens using flexural vibration,'' J. Acoust. Soc. Am. **100**, 2057–2061 (1996).

[2] B. T. Chu and R. E. Apfel, ''Acoustic radiation pressure produced by beam of sound,'' J. Acoust. Soc. Am. **72**, 1673–1687 (1982).

[3] C. P. Lee and T. G. Wang, ''Acoustic radiation pressure,'' J. Acoust. Soc. Am. **94**, 1099–1109 (1993).

[4] H. Nomura, T. Kamakura, and K. Matsuda, ''Theoretical and experimental examination of near-field acoustic levitation,'' J. Acoust. Soc. Am. **111**, 1578–1583 (2002).

[5] E. O. J. Salbu, ''Compressible squeeze films and squeeze bearings,'' J. Basic Eng. **86**, 355–366 (1964).

[6] A. Minikes and I. Bucher, ''Coupled dynamics of a squeeze-film levitated mass and a vibrating piezoelectric disc—numerical analysis and experimental study,'' J. Sound Vib. **263**(2), 241–268 (2003).

[7] Y. Hashimoto, Y. Koike, and S. Ueha, ''Transporting objects without contact using flexural travelling waves,'' J. Acoust. Soc. Am. **103**, 3230–3233 (1998).

[8] S. Ueha, Y. Hashimoto, and Y. Koike, ''Non-contacting transportation using near-field acoustic levitation,'' Ultrasonics **38**, 26–32 (2000).

[9] J. Hu, G. Li, H. L. W. Chan, and C. L. Choy, ''A standing wave-type nonconctact linear ultrasonic motor,'' IEEE Trans. Ultrason. Ferroelectr. Freq. Control **48**(3), 699–708 (2001).

[10] A. Minikes and I. Bucher, ''Noncontacting lateral transportation using gas squeeze film generated by flexural traveling waves-Numerical analysis,'' J. Acoust. Soc. Am. **113**, 2464–2473 (2003).

[11] W. E. Langlois, ''Isothermal squeeze films,'' Q. Appl. Math. **XX**(2), 131–150 (1962).

[12] W. A. Gross, *Gas Film Lubrication* (Wiley, New York, 1962).